
SINEKAN: KOLMOGOROV-ARNOLD NETWORKS USING SINUSOIDAL ACTIVATION FUNCTIONS *

Eric A. F. Reinhardt*

Department of Physics and Astronomy
The University of Alabama
Tuscaloosa, AL
eareinhardt@crimson.ua.edu

P. R. Dinesh

Department of Physics and Astronomy
The University of Alabama
Tuscaloosa, AL
dpr@crimson.ua.edu

Sergei Gleyzer

Department of Physics and Astronomy
The University of Alabama
Tuscaloosa, AL
sgleyzer@ua.edu

ABSTRACT

Recent work has established an alternative to traditional multi-layer perceptron neural networks in the form of Kolmogorov-Arnold Networks (KAN). The general KAN framework uses learnable activation functions on the edges of the computational graph followed by summation on nodes. The learnable edge activation functions in the original implementation are basis spline functions (B-Spline). Here, we present a model in which learnable grids of B-Spline activation functions are replaced by grids of re-weighted sine functions. We show that this leads to better or comparable numerical performance to B-Spline KAN models on the MNIST benchmark, while also providing a substantial speed increase on the order of 4-8 times.

1 Introduction

Multi-layer perceptrons (MLPs) are a fundamental component of many current leading neural networks [1, 2]. They are often combined with feature extracting tools, such as convolutional neural networks and multi-head attention, to create many of the best performing models, such as transformers [3, 4, 5, 6]. One of the key mechanisms that makes MLPs so powerful is that the layers typically end in non-linear activation functions which enables universal approximation from any arbitrary input space to any arbitrary output space using only a single sufficiently wide layer [7]. While MLPs enable any such arbitrary mapping, the number of neurons required to achieve that mapping can also be arbitrarily large.

Recent work [8] has presented an alternative to the MLP architecture, based on the Kolmogorov-Arnold Representation Theorem [9, 10, 11], accordingly denoted as Kolmogorov-Arnold Networks (KANs) [8]. In earlier seminal work, [9, 10], it was established that any arbitrary multivariate function can be approximated with a sum of continuous univariate functions over a single variable. In [8], it was shown that this approximation can be extrapolated to neural network architectures leading to competitive performance with MLPs at often significantly smaller model sizes [1][2]. In this work, we will use an efficient implementation of the KAN with learnable B-Spline activation functions (B-SplineKAN) [12] that is numerically consistent with the original implementation of KAN, but on the order of three to five times faster than the original implementation [8] for the purpose of performance comparison.

As Figure 1 shows, the order of operations in traditional MLPs is: on-edge weight multiplication, summation on node, addition of bias, followed by the application of the activation function. In KANs, the order of operations is:

**Citation:* E.A.F. Reinhardt¹, P.R. Dinesh, S. Gleyzer. SineKAN: Kolmogorov-Arnold Networks Using Sinusoidal Activation Functions.

¹Corresponding author.

learnable activation function on edge, summation on node and optional addition of bias on node. This alternative order of operations satisfies the Kolmogorov-Arnold Representation Theorem and can potentially allow significantly smaller computational graphs compared to MLPs [8].

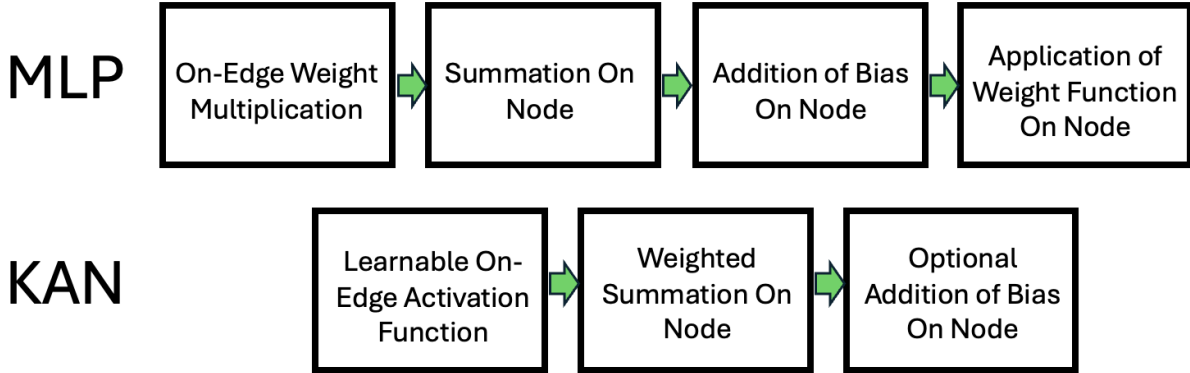


Figure 1: Flow of operations. Top: MLP Bottom: KAN

The work establishing KAN as a viable model [8] explored the use of B-Splines as the learnable activation function. There is a strong motivation for the choice of B-Splines. Using B-Splines, it is possible to change the size of layer’s grid of spline coefficients without meaningfully affecting the model itself, enabling downstream fine-tuning. It is also possible to sparsify the model through a process of pruning low-impact spline terms. It is additionally possible to determine the functional form of the model symbolically. [8] found that B-Spline models achieved competitive results with MLP layers on a broad range of tasks. The choice of B-Splines isn’t without its costs however, as B-SplineKAN layers are significantly slower than MLPs and, while recent implementations have helped to close the gap, MLPs are still substantially faster. Furthermore, there are many tasks presented in [8] where MLPs still outperformed the B-SplineKAN. Recent work has shown that alternatives to B-SplineKAN can achieve competitive performance under fair comparison [13].

A number of alternative univariate functions to B-Splines have been explored for use in KANs, including wavelets [14], Chebyshev polynomials [15], fractional functions [16], rational Jacobi functions [17], radial basis functions [18], and even variations on Fourier expansions [19], discussed in detail in Section §2.2. In this paper we present SineKAN, a KAN implementation with sine activation functions.

Periodic activation functions in neural networks have been explored extensively and shown to provide strong approximations for a broad class of problems [20, 21, 22, 23, 24]. Work using sinusoidal representational networks [25] has shown that sinusoidal activation functions lead to strong performance on problems with continuous domains [26] and potentially discontinuous domains [27, 28]. These promising results in sinusoidal activations motivate sine functions as a potentially strong alternative to other explored activation functions for KANs.

In Section §2 we describe the SineKAN architecture, whether it satisfies a universal approximation, and outline a weight initialization strategy that scales consistently with differing grid sizes and stabilizes numerical performance across multi-layer models. In Section §3, we present results of model inference speed and performance on the MNIST benchmark and compare it with B-SplineKAN implementation. We discuss our results in Section §4 and summarize our findings in Section §5.

2 SineKAN

2.1 Sinusoidal Activation Function

Here, we propose an alternative to the B-SplineKAN architecture described in Section §1 that is based on sine functions. Mathematically each layer can be expressed as:

$$y_i = \sum_j \sum_k (\sin(x_j * \omega_k + \phi_{jk}) * A_{ijk}) + b_i \quad (1)$$

where y_i are the layer output features, x_j are the layer input features, ϕ_{jk} is a phase shift over the grid and input dimensions, ω_k is a grid frequency, w_{ijk} are the amplitude weights, and b_i is a bias term. The base functional form

of the sines are fixed, while the functional form of the sine activations is learned through learnable frequency and amplitude terms performed over a grid of fixed phases.

2.2 Grid Phase Shift

In previous work using Fourier series, KAN networks use the form of a full Fourier series expansion, denoted as the following[19]:

$$y_i = \sum_j \sum_k (\sin(x_j * w_{ijk}) + \cos(x_j * v_{ijk}) + b_i) \quad (2)$$

Here there is an additional weight matrix v_{ijk} compared to our solution:

$$y_i = \sum_j \sum_k (\sin(x_j * \omega_k + \phi_{jk}) * A_{ijk}) + b_i \quad (3)$$

By introducing learnable frequencies ω_k over a grid with fixed phase shifts ϕ_{jk} and input dimensions, we reduce the number of learnable parameters from $O(2oig)$ to $O(oig + g)$ where o is the output dimension, i is in the input dimension, and g is the grid size. We show later in §2.4 that this still satisfies universal approximation.

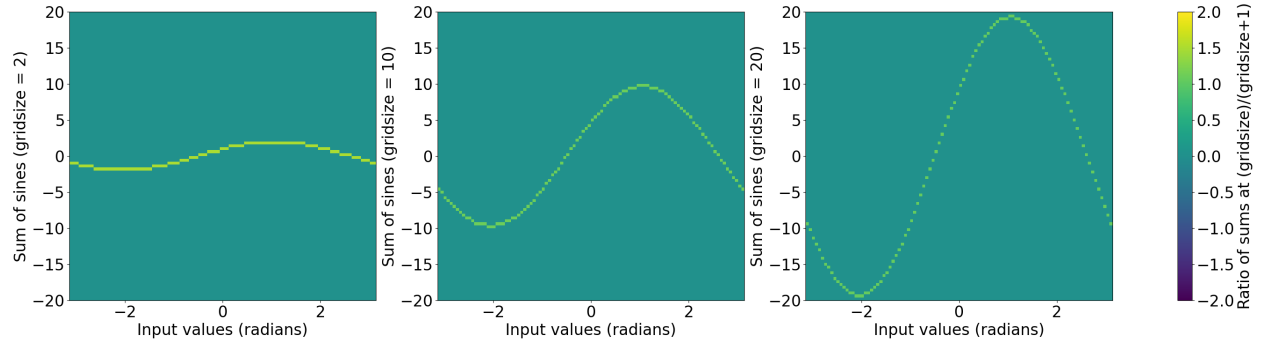


Figure 2: Value of $\sum_{i=1}^g \sin(x + i * \pi / (g + 1))$ as a function of x with the ratio of sum at $g+1$ over the sum at g as the color scale. Left to right: $g=2$, $g=10$, $g=20$.

Under the initial assumption for the first layer of the model, a naive approach for initializing the grid weights is to cover a full phase shift range, where the grid phase shift terms would be a range of values from 0 to π . However, it can be shown that, for the following case:

$$\sum_{i=1}^g \sin(x + i * \pi / g) \quad (4)$$

where g is the grid size, the total sum increases non-linearly as a function of g . Most importantly, the total sum is independent of input value, x . This makes finding the appropriate grid weight scaling inconsistent across types of inputs and grid dimension. We present an alternative strategy, in which grid weights are initialized as:

$$\sum_{i=1}^g \sin(x + i * \pi / (g + 1)) \quad (5)$$

As Figure 2 shows, this stabilizes the scaling ratio between consecutive grid sizes across arbitrary input values.

Furthermore, we find that introducing an additional input phase term along the axis of the number of input features with values ranging from zero to π leads to stronger model performance.

Finally, to stabilize the model scaling across different grid sizes, we find a functional form that helps scale the total sum across the grid dimension as a ratio of phase terms:

$$R = A * g^{-K} + C \phi_{g+1} = \phi_g * R(g) \quad (6)$$

where $A = 0.97241$, $K = 0.988440$ and $C = 0.999450$, R is a scale factor by which all phase terms are multiplied as you increase from a grid size of one upward, and ϕ_g is the phase at a particular grid size. To determine A , K , and C we perform least squares minimization of:

$$L(g, x) = \sigma^2(f(g + 1, x)/f(g, x)) + (1 - \mu(f(g + 1, x)/f(g, x)))^2 \tag{7}$$

where L is a cost function, $f(g, x)$ is the sum of sines across input values from $-\pi$ to π .

Using this functional form we can initialize layers with arbitrary grid sizes by using the exponential expression in a recursive formula while initializing the grid phase weights. The resulting ratios of sums of sines are shown in Figure 3.

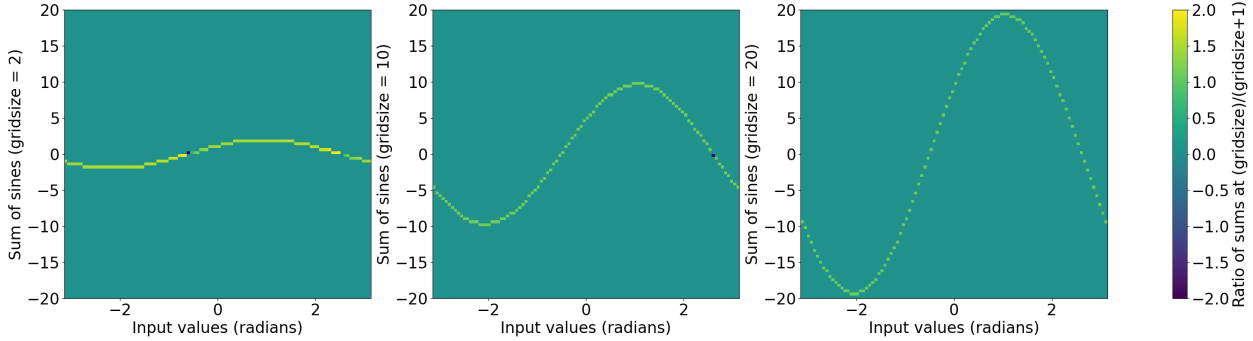


Figure 3: $\sum_{i=1}^g \sin(x + i * \pi / (g + 1) * R(g))$ with the ratio of sum at $g+1$ over the sum at g as the color scale. Left to right: $g=2, g=10, g=20$.

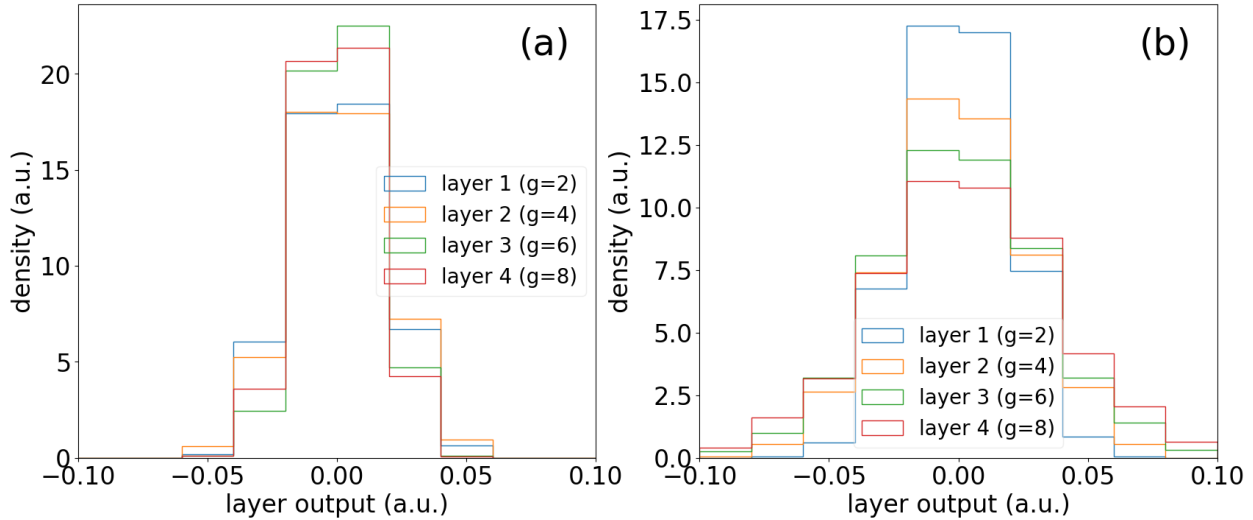


Figure 4: (a) Outputs of layers of same size ($N=1000$) with the recursive function applied for grid size scaling. (b) Outputs of layers of same size ($N=1000$) without the recursive function applied for grid size scaling.

In Figure 4(b), we see the outputs of subsequently connected layers when recursive grid size phase scaling is not applied. In Figure 4(a), we see the same scenario but with recursive grid size phase scaling applied and see an increase in similarity of layer outputs across various grid sizes.

2.3 Scaling of Phase Terms With Grid Size

We find a weight initialization strategy which results in strong performance and stability in higher depth models. For the first layer, the weights are initialized as a random distribution with a mean of 0 and a standard deviation of 0.4 and for the subsequent layers, the weights are initialized from a uniform distribution between -1 and 1. This not only leads to consistent layer weight distributions, but also leads to consistent output across connected layers of same size, as shown in Figure 5(b).

It also features a desirable property that, given a fixed initialization on the first layer and a random input vector, the features span a broader range of values at deeper layers, as shown in Figure 5(a). This implies that no value collapse

is introduced. Comparatively, we see in Figure 5(c), that the model layer outputs in B-SplineKAN implementations decrease in multi-layer models, which can play a significant role in results in Section §3.1.

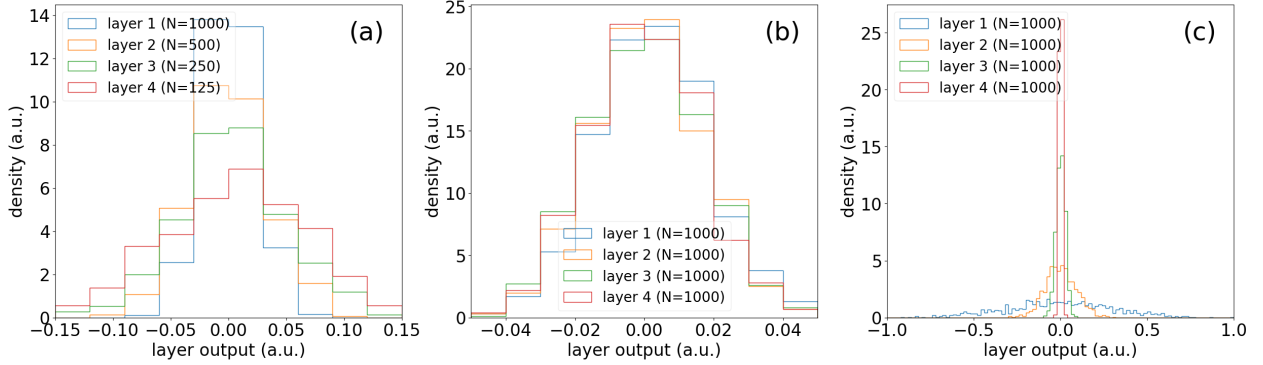


Figure 5: (a) Outputs of consecutive layers of different sizes in a SineKAN model. (b) Outputs of consecutive layers of same size in a SineKAN model. (c) Outputs of consecutive layers of same size in a B-SplineKAN model.

2.4 Universal Approximation

The combination of learnable amplitudes and sinusoidal activation functions have previously been explored [25, 27, 28, 26]. However, these models only satisfy universal approximation on a single layer when combined with linear transformations in sufficiently wide or deep models. By introducing an additional degree of freedom in the form of learnable frequencies over phase-shifted grids, one can eliminate the linear transformation layers.

Any sufficiently well-behaved/smooth 1 dimensional function $f : \mathbb{R} \rightarrow \mathbb{R}$ can be expressed in terms of a *Fourier transform* $\tilde{f} : \mathbb{R} \rightarrow \mathbb{C}$ w.r.t. a continuous phase space of frequencies ω :

$$\begin{aligned}
 f(x) &= \int_{\mathbb{R}} d\omega \tilde{f}(\omega) e^{i\omega x} \\
 &= \text{Re} \left(\int_{\mathbb{R}} d\omega \tilde{f}(\omega) e^{i\omega x} \right) \\
 &= \int_{\mathbb{R}} d\omega A(\omega) \cos(\omega x + \phi'(\omega)) \\
 &= \int_{\mathbb{R}} d\omega A(\omega) \sin(\omega x + \phi(\omega))
 \end{aligned}$$

where $A(\omega)$ and $\phi(\omega) = \phi'(\omega) - \frac{\pi}{2}$ are real-valued functions. The above integral can be discretized using Riemannian sums over a finite set of frequencies $\Omega = \{\omega_1, \omega_2 \dots \omega_G\}$ where cardinality G of the set is the *grid size*. We henceforth propose the following variational function g_θ as an ansatz for $f(x)$:

$$g_\theta(x) = \sum_i B_i \sin(\omega_i x + \phi_i)$$

where we make the replacements $\int_{\mathbb{R}} \rightarrow \sum_i$, $d\omega A(\omega) \rightarrow B_i$ and $\omega, \phi(\omega) \rightarrow \omega_i, \phi_i$. Here, ϕ_i are G fixed, finite points from $(0, \pi + 1]$ while we treat all other subscripted symbols B_i, ω_i as weights whose values can be trained to optimize a loss function between f and g_θ , which converges to the Fourier transform integral of f as $G \rightarrow \infty$. Hence, in the limit where $G \rightarrow \infty$, it's a valid candidate for a learnable activation function ansatz to be used in a Kolmogorov-Arnold network (KAN).

In 6 we show that with a layer with grid size of 100, a single-input, single-output SineKAN layer can map inputs to outputs in 1D functions including over non-smooth functional mappings.

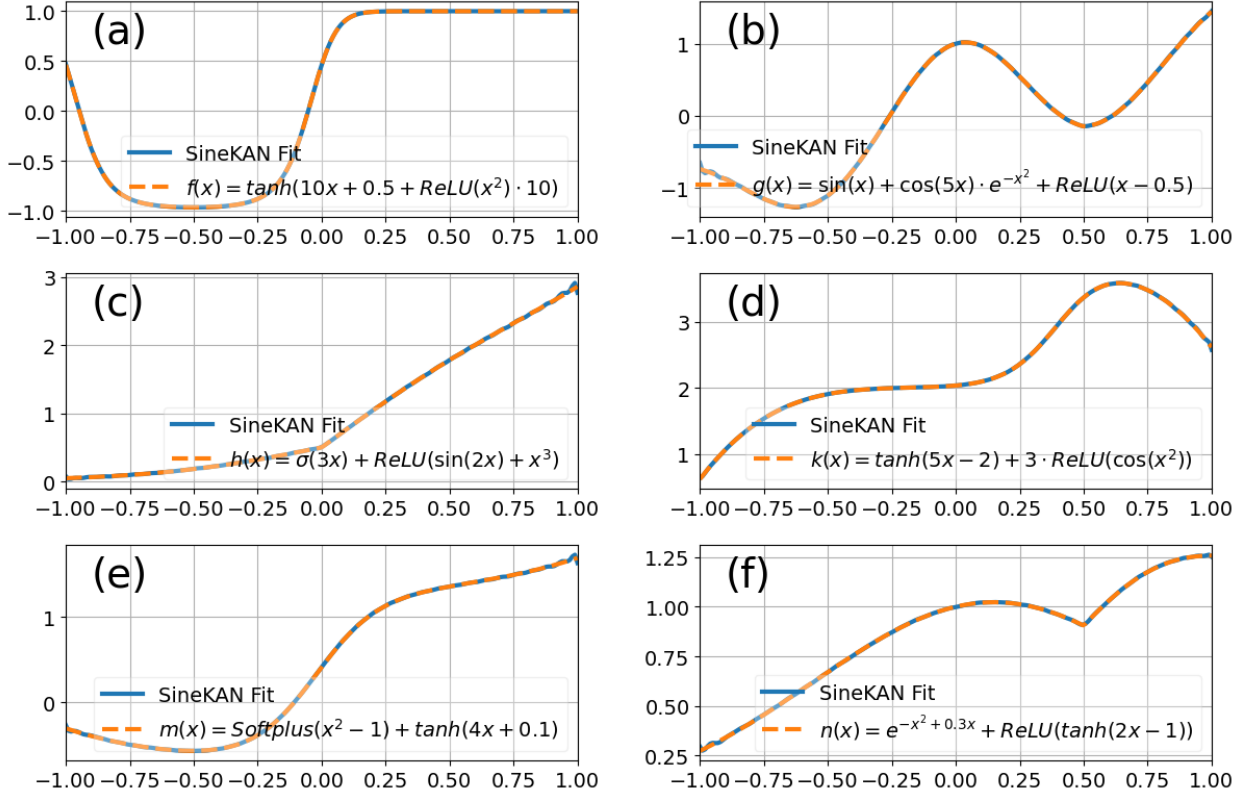


Figure 6: Fits of SineKAN with grid size of 100 to assorted functions. (a) $f(x) = \tanh(10x + 0.5 + \text{ReLU}(x^2) \cdot 10)$, (b) $g(x) = \sin(x) + \cos(5x) \cdot e^{-x^2} + \text{ReLU}(x - 0.5)$, (c) $h(x) = \sigma(3x) + \text{ReLU}(\sin(2x) + x^3)$, (d) $k(x) = \tanh(5x - 2) + 3 \cdot \text{ReLU}(\cos(x^2))$, (e) $m(x) = \text{Softplus}(x^2 - 1) + \tanh(4x + 0.1)$, (f) $n(x) = e^{-x^2 + 0.3x} + \text{ReLU}(\tanh(2x - 1))$

3 Results

3.1 Numerical Performance on MNIST

We train and compare single-layer B-SplineKAN and SineKAN networks on the MNIST dataset [29]. We use a batch size 128, learning and decay rates of 0.9 and learning rates of $5e-3$ for B-Spline and $4e-4$ for SineKAN, optimized with grid search. The models are trained using the AdamW optimizer with a weight decay of 0.01 for B-SplineKAN and 0.5 for SineKAN also found via grid search [30]. We test model performance with single hidden layer dimensions of 16, 32, 64, 128, 256, 512 training for 30 epochs using cross entropy loss [31].

Hidden Layer Size	16	32	64	128	256	512
B-SplineKAN	0.9577	0.9730	0.9783	0.9835	0.9826	0.9834
SineKAN	0.9618	0.9767	0.9819	0.9851	0.9854	0.9860

Table 1: Comparison of B-SplineKAN and SineKAN across different sample sizes

Fig. 7 shows the model validation accuracy as a function of the number of epochs. The best accuracies are shown in Table 1. The SineKAN model achieves better results than the B-SplineKAN model for all hidden layer sizes.

We additionally explore fitting using the same hyperparameters but with 1, 2, 3, and 4 hidden layers of size 128. Figure 8 shows that the SineKAN outperforms the B-SplineKAN at lower layer depths. Additionally, the SineKAN model accuracy predictably decreases at higher depths with same hyperparameters while the B-SplineKAN validation accuracy erratically varies at higher depths.

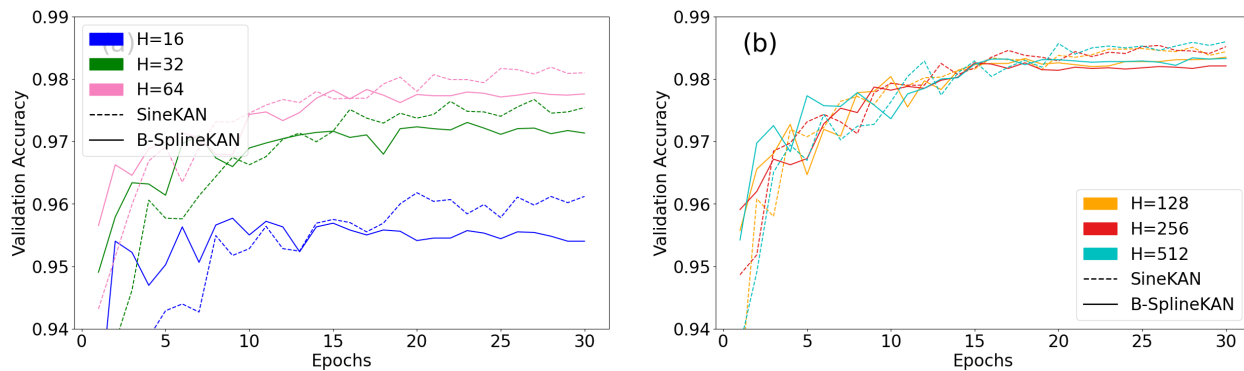


Figure 7: Validation accuracy of B-SplineKAN and SineKAN on MNIST with a single hidden layer of size (a) 16, 32, 64 and (b) 128, 256, 512.

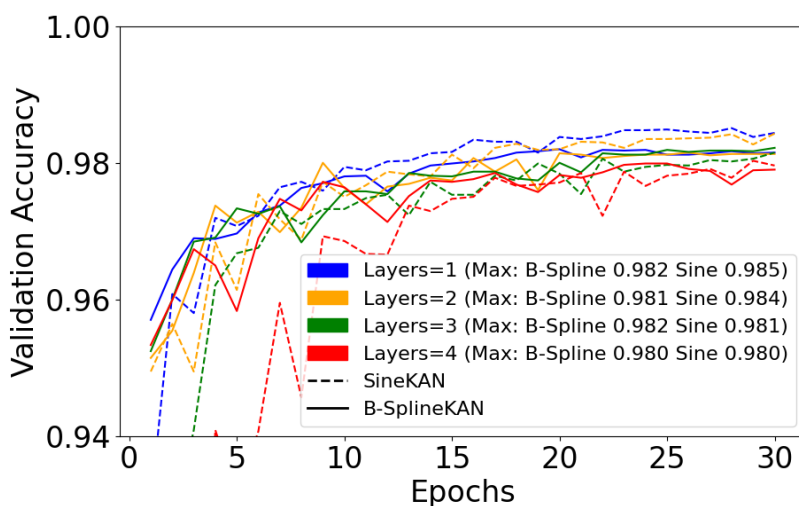


Figure 8: B-SplineKAN and SineKAN validation accuracy on MNIST with a 1, 2, 3, and 4 hidden layers of size 128.

3.2 Model Inference Speeds

We benchmark the speed of SineKan and B-SplineKAN models using NVIDIA T4 GPU with 16GB of RAM. We test performance on variable batch sizes of 16, 32, 64, 128, 256, 512 on single inputs of 784 features using a single hidden layer of size 128 with a grid size of 8. We test performance on single hidden layer hidden dimensions of 16, 32, 64, 128, 256, 512 under the same conditions. We test performance with single batch of 784 features with 1, 2, 3, and 4 hidden layers of size 128.

As Figure 9 shows, the SineKAN has better inference times at all batch sizes and scales better with larger batch sizes, ranging from 4.29 times faster at a batch size of 16 to 8.10 times faster a batch size of 512. While substantially faster at all batch sizes explored, the SineKAN model scales slightly worse with hidden layer size, ranging from around 8.09 at a layer size of 16 to 5.73 times faster at a layer size of 512. Finally, the SineKAN scales slightly better with number of layers, at 6.49 times faster for a depth of one hidden layer and 7.14 times faster for a depth of four hidden layers.

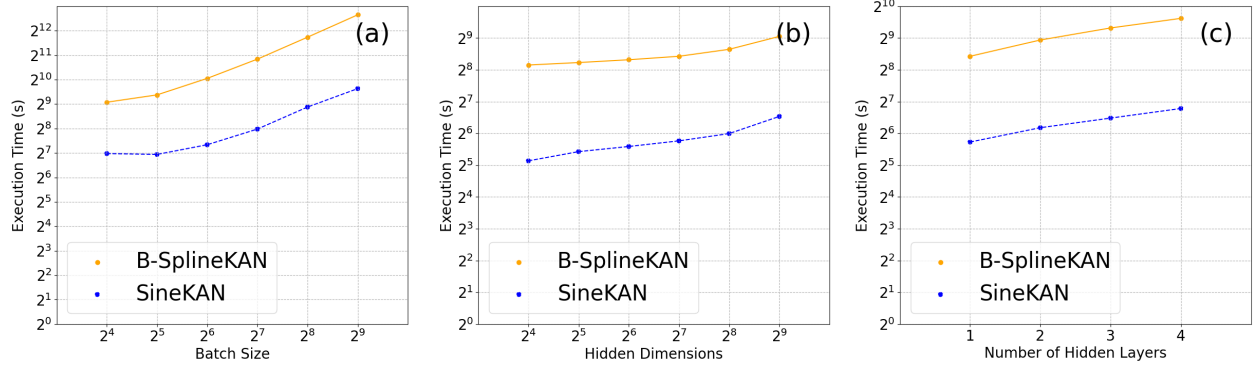


Figure 9: Average inference times (averaged over 1000 passes) of B-SplineKAN and SineKAN run on NVIDIA Tesla T4 GPU (16GB RAM) with (a) One layer of size 128 with grid size of 8 on input data with 784 features with batch sizes of 16, 32, 64, 128, 256, 512. (b) One layer of sizes 16, 32, 64, 128, 256, 512 with grid size of 8 on a single input with 784 features. (c) 1, 2, 3, and 4 hidden layers of sizes 128 with grid size of 8 on a single input with 784 features.

4 Discussion

The SineKAN model, which uses sine functions as an alternative to existing baseline B-Spline activation functions [8], shows very good performance on the benchmark task. Model stabilization techniques described in Section §2.2 lead to consistent model layer output weights at different depths and sizes of phase shift grids. We also show that it actively mitigates value collapse in deep models.

In Section §3.1, we show that our model increasingly outperforms the B-SplineKAN model at very large hidden layer dimensions. These results suggest that the SineKAN model may be a better choice compared to B-SplineKAN for scalable, high-depth, large batch models such as large language models (LLMs).

We show in Section §3.2 that the SineKAN model is on the order of 4 to 8 times faster than an efficient implementation of B-SplineKAN [12] under similar circumstances with better scaling for deep models over large batch sizes. However, while still substantially faster at all hidden layer sizes explored, the scaling is slightly worse than B-SplineKAN for large hidden layer sizes. This can largely be attributed to large memory overhead in the B-SplineKAN operations even at small hidden layer sizes, however, this is worth future exploration.

We also found that SineKAN had a significantly different optimal learning rate and weight decay compared to B-SplineKAN which motivates the idea that a fair comparison cannot be done across different KAN implementations without performing a grid search to find optimal hyperparameters. Further, we also showed in Section §2.3, that B-SplineKAN has an inherent flaw in scaling to multi-layer models in that it increasingly constricts layer outputs at higher depths. This likely necessitates additional layer normalization between B-SplineKAN layers. We recommend that approaches for stabilizing model weights at different sizes and depths, similar to those outlined in §2.3 and §2.2, should be employed in other KAN models to improve deep model stability and performance.

In summary, sinusoidal activation functions appear to be a promising candidate in the development of Kolmogorov-Arnold models. SineKAN has superior performance in inference speed and accuracy, as well as multi-layer scaling when compared with B-SplineKAN. However, a number of other activation functions mentioned in Section §1 have also shown to have superior inference speed and better numerical performance. Further exploration is needed to compare the performance both in terms of inference speed and numerical performance on the broad range of KAN implementations, and on a broader range of tasks, under fair conditions.

5 Conclusion

We present the SineKAN model, a sinusoidal activation function alternative to B-SplineKAN Kolmogorov-Arnold Networks. We find that this model leads to better numerical performance on the MNIST benchmark task, when both models are trained using near-optimal hyperparameters found with a parameter grid search. The SineKAN model outperforms B-SplineKAN at higher hidden dimension sizes with more predictable performance scaling at higher depths. We further find that our model outperforms efficient implementations of B-SplineKAN on speed benchmarks by a factor of four to nine times with better scaling across batch size.

6 Code

The SineKAN code can be found at <https://github.com/ereinha/SineKAN>.

7 Acknowledgements

This work was supported by the U.S. Department of Energy (DOE) under Award No. DE-SC0012447 (E.R. and S.G.). E.R. was a participant in the 2023 Google Summer of Code Program.

References

- [1] David E. Rumelhart, James L. McClelland, and CORPORATE PDP Research Group, editors. *Parallel distributed processing: explorations in the microstructure of cognition, vol. 1: foundations*. MIT Press, Cambridge, MA, USA, 1986.
- [2] David E Rumelhart, Geoffrey E Hinton, and Ronald J Williams. Learning representations by back-propagating errors. *nature*, 323(6088):533–536, 1986.
- [3] Y. LeCun, B. Boser, J. S. Denker, D. Henderson, R. E. Howard, W. Hubbard, and L. D. Jackel. Backpropagation applied to handwritten zip code recognition. *Neural Computation*, 1(4):541–551, 1989.
- [4] Y. Lecun, L. Bottou, Y. Bengio, and P. Haffner. Gradient-based learning applied to document recognition. *Proceedings of the IEEE*, 86(11):2278–2324, 1998.
- [5] Ashish Vaswani, Noam Shazeer, Niki Parmar, Jakob Uszkoreit, Llion Jones, Aidan N. Gomez, Lukasz Kaiser, and Illia Polosukhin. Attention is all you need. *CoRR*, abs/1706.03762, 2017.
- [6] Kaiming He, Xiangyu Zhang, Shaoqing Ren, and Jian Sun. Deep residual learning for image recognition, 2015.
- [7] K. Hornik, M. Stinchcombe, and H. White. Multilayer feedforward networks are universal approximators. *Neural Netw.*, 2(5):359–366, jul 1989.
- [8] Ziming Liu, Yixuan Wang, Sachin Vaidya, Fabian Ruehle, James Halverson, Marin Soljačić, Thomas Y. Hou, and Max Tegmark. Kan: Kolmogorov-arnold networks, 2024.
- [9] A. N. Kolmogorov. On the representation of continuous functions of several variables as superpositions of continuous functions of a smaller number of variables. *Doklady Akademii Nauk*, 108(2), 1956.
- [10] Andrei Nikolaevich Kolmogorov. On the representation of continuous functions of many variables by superposition of continuous functions of one variable and addition. In *Doklady Akademii Nauk*, volume 114, pages 953–956. Russian Academy of Sciences, 1957.
- [11] Jürgen Braun and Michael Griebel. On a constructive proof of kolmogorov’s superposition theorem. *Constructive Approximation*, 30:653–675, 2009.
- [12] Huanqi Cao. Efficient-kan, 2024. Accessed: 2024-06-27.
- [13] Khemraj Shukla, Juan Diego Toscano, Zhicheng Wang, Zongren Zou, and George Em Karniadakis. A comprehensive and fair comparison between mlp and kan representations for differential equations and operator networks, 2024.
- [14] Zavareh Bozorgasl and Hao Chen. Wav-kan: Wavelet kolmogorov-arnold networks, 2024.
- [15] Sidharth SS, Keerthana AR, Gokul R, and Anas KP. Chebyshev polynomial-based kolmogorov-arnold networks: An efficient architecture for nonlinear function approximation, 2024.
- [16] Alireza Afzal Aghaei. fkan: Fractional kolmogorov-arnold networks with trainable jacobi basis functions, 2024.
- [17] Alireza Afzal Aghaei. rkan: Rational kolmogorov-arnold networks, 2024.
- [18] Hoang-Thang Ta. Bsrbf-kan: A combination of b-splines and radial basic functions in kolmogorov-arnold networks, 2024.
- [19] Jinfeng Xu, Zheyu Chen, Jinze Li, Shuo Yang, Wei Wang, Xiping Hu, and Edith C. H. Ngai. Fourierkan-gcf: Fourier kolmogorov-arnold network – an effective and efficient feature transformation for graph collaborative filtering, 2024.
- [20] R. Gallant and H. White. There exists a neural network that does not make avoidable mistakes. In *IEEE International Conference on Neural Networks*, pages 657–664, 1988.

- [21] Abylay Zhumekenov, Malika Uteuliyeva, Olzhas Kabdolov, Rustem Takhanov, Zhenisbek Assylbekov, and Alejandro J. Castro. Fourier neural networks: A comparative study. *arXiv preprint arXiv:1902.03011*, 2019.
- [22] Josep M. Sopena, Enrique Romero, and Rene Alquezar. Neural networks with periodic and monotonic activation functions: a comparative study in classification problems. In *Proc. ICANN*, 1999.
- [23] Kwok wo Wong, Chi sing Leung, and Sheng jiang Chang. Handwritten digit recognition using multilayer feedforward neural networks with periodic and monotonic activation functions. In *Object recognition supported by user interaction for service robots*, volume 3, pages 106–109. IEEE, 2002.
- [24] Giambattista Parascandolo, Heikki Huttunen, and Tuomas Virtanen. Taming the waves: Sine as activation function in deep neural networks. 2016.
- [25] Vincent Sitzmann, Julien N. P. Martel, Alexander W. Bergman, David B. Lindell, and Gordon Wetzstein. Implicit neural representations with periodic activation functions, 2020.
- [26] Minjie Lei, Ka Vang Tsang, Sean Gasiorowski, Chuan Li, Youssef Nashed, Gianluca Petrillo, Olivia Piazza, Daniel Ratner, and Kazuhiro Terao. Implicit neural representation as a differentiable surrogate for photon propagation in a monolithic neutrino detector, 2022.
- [27] Sebastien Origer and Dario Izzo. Guidance and control networks with periodic activation functions, 2024.
- [28] Yamin Li, Ange Lou, Ziyuan Xu, Shiyu Wang, and Catie Chang. Leveraging sinusoidal representation networks to predict fmri signals from eeg, 2024.
- [29] Li Deng. The mnist database of handwritten digit images for machine learning research. *IEEE Signal Processing Magazine*, 29(6):141–142, 2012.
- [30] Ilya Loshchilov and Frank Hutter. Decoupled weight decay regularization, 2019.
- [31] David E Rumelhart, Geoffrey E Hinton, and Ronald J Williams. Learning representations by back-propagating errors. *nature*, 323(6088):533–536, 1986.